Corresponding author:

Dr. Rosie Boltryk

School of Engineering Sciences

University of Southampton

Southampton

SO17 1BJ, UK

Telephone: +44 (0) 238059 2896

Fax: +44 (0) 238059 7322

Email: R.J.Boltryk@soton.ac.uk

(ICU'2009/Martyn_Hill)
Multi-modal particle manipulator to enhance bead-based bioassays

P. Glynne-Jones[1], R. J. Boltryk[1], M. Hill.[1], F. Zhang[2], L. Dong[2], J. S. Wilkinson[2], T. Brown[3], T. Melvin[2], N. R. Harris[4]

[1]School of Engineering Sciences, University of Southampton, SO17 1BJ, UK

[2] Optoelectronics Research Centre, University of Southampton, SO17 1BJ, UK

[3] School of Chemistry, University of Southampton, SO17 1BJ, UK

[4] School of Electronics and Computer Science, University of Southampton, SO17 1BJ, UK

Abstract: By sequentially pushing micro-beads towards and away from a sensing surface, we show that ultrasonic radiation forces can be used to enhance the interaction between a functionalized glass surface and polystyrene micro-beads, and identify those that bind to the surface by illuminating bound beads using an evanescent field generated by guided light.

The movement towards and immobilization of streptavidin coated beads onto a biotin functionalized waveguide surface is achieved by using a quarter-wavelength mode pushing beads onto the surface, while the removal of non-specifically bound beads uses a second quarter-wavelength mode which exhibits a kinetic energy maximum at the boundary between the carrier layer and fluid, drawing beads towards this surface. This has been achieved using a multi-modal acoustic device which exhibits both of these quarter-wavelength resonances. Both 1-D acoustic modelling and finite element analysis has been used to design this device and to investigate the spatial uniformity of the field.

We demonstrate experimentally that 90% of specifically bound beads remain attached after applying ultrasound, with 80% of non-specifically bound control beads being successfully removed acoustically. This approach overcomes problems associated with lengthy sedimentation processes used for bead-based bioassays and surface (electrostatic) forces, which delay or prevent immobilisation. We explain the potential of this technique in the development of DNA and protein assays in terms of detection speed and multiplexing.

PACS code: 43.90 v

Key words: acoustic radiation forces, bio-sensor, frequency switching, micro-beads, optical waveguide.

1 Introduction

Bead-based assays are becoming increasingly important in microfluidic sensor systems with the advantage that the bead surface forms a disposable sensing element and a high bead surface area coupled with active mixing. These assays may be realised using magnetic beads held in devices using magnetic forces [1], however acoustic radiation forces can be used to manipulate a wider range of beads, including magnetic and non-magnetic beads, as they rely on acoustic properties only. The approach also allows finer control over bead position. Despite the advantages that acoustically enhanced bioassays could bring, it remains a challenge to move beads consistently to the detection area and in a uniform pattern. Thus a thorough understanding of the 2-D nature of the acoustic field in such a system is needed to ensure that beads can be suitably controlled. In this paper we investigate the axial acoustic field distribution using a 1-D acoustic impedance transfer model [2], and also finite element analysis to model the lateral variation of the field. Thus the uniformity and suitability of the 2-d field may be judged. To aid this assessment a simulation of force potential, $\langle \phi(r) \rangle$, is used to provide a means of predicting bead migration.

2 Device Design

2.1 General

In order to enhance bead-based assays, it is proposed that acoustic radiation forces are used to a) push beads to the detection surface and b) discriminate between beads that bind to the surface and those that do not by subsequently repelling unbound beads. Fig.1 illustrates two acoustic modes which provide these two functions. Firstly, Fig.1(a) shows a “to-reflector” quarter-wave mode, used to move beads to the detection surface and secondly Fig.1(b) shows a “to-carrier” quarter-wave mode, used to force beads off the surface. In both cases, there must be sufficient radiation force at the wall to enhance binding and to overcome surface forces, which dictates where pressure nodes and antinodes are positioned in relation to the surface (noting that radiation force is typically zero at these nodal points). Fig.1 therefore also indicates how the “to-carrier” nodal points have been positioned some way into the reflector surface to ensure that beads are forced onto the surface.

2.2 Transfer Impedance 1-D Model

The final design was arrived at through successive iterations, investigating the behaviour as predicted by a 1-D transfer impedance model [2] implemented in MATLAB. This represents the structure as a layered resonator with layers of infinite lateral extent, thus ignoring any lateral acoustic modes.

This is sufficiently accurate, however, to arrive at a suitable multi-modal design. The transducer representation used by Hill et al. [2] was replaced by a KLM circuit model [3] extending the operating frequency of the model beyond the

first resonance. For each design iteration, the average acoustic energy density (see equations below) in the fluid layer versus frequency is inspected; this allows all the resonances supported by that configuration to be identified and examined to determine their resultant acoustic force potential. Of the modes described in Fig.1, the reflector quarter-wave mode is found to be the most sensitive to geometry, so it was easier to start the process with a design that easily supported this mode, with subsequent changes aiming to enhance the strength of the carrier layer quarter-wave mode.

These design iterations produced the final design depicted in Fig. 2, whose layer thicknesses are recorded in Table 1. The chamber floor is formed from macor, a machinable ceramic, with a PZT transducer (a 10mm diameter disc of PZT26, Ferroperm,) glued (Epotek 301 epoxy) to the reverse side. The walls of the fluidic chamber (chamber 5mm in diameter) are formed by a moulded PDMS gasket to prevent the steel spacer coming into fluidic contact with the sample, and also to reduce the strength of lateral acoustic modes that cause variations in the radiation force across the width of the device. The roof of the chamber (the acoustic reflector) is formed by a sheet of BK7 glass. Fluidic connections are supplied via a PMMA manifold which connects to the fluidic chamber via ports in the macor layer, with PDMS gaskets to seal the connection. An aluminium clamp holds the assembly together. The ultrasonic transducer is powered by an RF-amplifier (ENI 240L) driven by a sine-wave from a signal generator (TTi TG1304).

Troughs in the resulting modelled impedance data are indicative of a resonance and clearly show two modes (Fig. 3), the peaks in the acoustic energy density in the fluid confirm that they are resonances directly associated or coupled with the fluid layer. These correspond to the carrier quarter-wave and reflector quarter-wave modes which are located at 1.57 and 1.70MHz respectively. The smaller energy density associated with the reflector quarter-wave mode is indicative of the design challenge that this mode presents.

2.3 Finite Element (FE) Model

In order to gain a more detailed understanding of the behaviour of the device, including lateral forces, an axisymmetric finite element model was implemented using the ANSYS package.

2.3.1 Construction of Model

The modelling of lateral fields has been described by Neild et al. [4], Manneberg et al. [5], Lilliehorn et al. [6], Hagsater et al. [7] and Townsend et al. [8], and this work extends that of Townsend, incorporating a finite element representation of the transducer and using the results to visualise the force distribution in three-dimensions. Even in layered resonator designs which are most suited to a one-dimensional approach, significant lateral variations in acoustic radiation forces can be observed [8], which finite element analysis could be used to model.

A full verification of this Finite Element approach is beyond the scope of this paper, but Fig.4 represents some initial verification: it compares the transfer impedance model to a finite element model with boundary conditions set to

mimic layers of infinite extent. The finite element model is based in ANSYS [9], and uses a strip of FLUID29 (2-D harmonic acoustic) elements; carrier and reflector layers are represented by 2-D structural solid elements, PLANE42; and the PZT by the piezoelectric formulation of the 2-D Coupled-Field Solid PLANE13. Varying the parameters of the transmission line model, it is found that for the parameters considered here, the air beyond the reflector and transducers has little effect on the energy density profile, and is not included in the ANSYS model. The acoustic fluid elements are not formulated to allow any fluid damping in the fluid body, which makes predictions of acoustic amplitudes less accurate, particularly for half-wave devices where the fluid damping is important, however in the future, other element types such as FLUID79 which can include fluid damping will be explored in the future. All materials data is taken from manufacturers' data tables. The figure contains two maxima in the time averaged fluid energy density corresponding to the 'to carrier' and 'to reflector' quarter wave modes. It can be seen that there is good agreement between the two types of model.

For the axisymmetric model shown in Fig.5, the same element types were used; the additional spacer layer was also represented by PLANE42 elements. The dimensions of the model are as listed in Table 1, the radius of the modelled reflector and carrier layer was 80mm and the transducer radius 25mm; the spacer as an annulus of inner and outer radii 50mm and 80mm respectively. The region between the fluid and the spacer is physically composed of a PDMS gasket and some air spaces; in order to mimic the energy scattering nature of this region (to acoustic energy from the fluid), the right-side of the fluid layer is bounded by a 50% absorbing boundary condition with the remaining space left as a void in the model, as it is anticipated that the gasket and air will have little effect on the dynamics of the surrounding material.

2.3.2 Calculation of force potential

For a harmonically varying sound field, where the fluid particle velocity, *u*, has amplitude *U* and fluid pressure, *p*, has amplitude *P*, the time averaged kinetic and potential energy densities can be calculated [10] as

$$\left\langle \overline{E}_{kin}(r) \right\rangle = \frac{1}{4}\rho_0 U^2, \qquad (1)$$

and

$$\left\langle \overline{E}_{pot}(r) \right\rangle = \frac{1}{4}\frac{P^2}{\rho_0 c^2}, \qquad (2)$$

where ρ_0 is the density of the fluid, and *c* the speed of sound in the fluid.

Post processing of the FLUID29 *u* and *p* output parameters allows these equations to be implemented. The following equations derived by Gor'kov [11] allow the radiation force to be derived from an arbitrary standing wave

field and the acoustic potential and energy densities. The acoustic radiation force (a time averaged quantity) is given by [12]

$$\langle F(r)\rangle = -\nabla\langle\phi(r)\rangle, \qquad (3)$$

where the force potential, $\langle\phi(r)\rangle$, is given by

$$\langle\phi(r)\rangle = -V\left[\frac{3(\lambda-1)}{2\lambda+1}\langle\overline{E}_{kin}(r)\rangle - \left(1-\frac{1}{\sigma^2\lambda}\right)\langle\overline{E}_{pot}(r)\rangle\right], \qquad (4)$$

and where λ is the ratio of particle density to fluid density, σ the ratio of speed of sound in the particle to that in the fluid and V the particle volume.

2.3.3 Simulation results

Plotting the acoustic force potential, $\langle\phi(r)\rangle$, is a convenient way of visualising the acoustic forces. A particle will tend to move towards regions where $\langle\phi(r)\rangle$ is low (indicated black in Fig.6) with a force proportional to the spacings of plotted contour lines.

Fig.6 shows the force potential in the fluid for three modes, where the left boundary represents the centre of the chamber and right boundary the gasket wall (fluid elements shown in Fig.5). The frequencies at which these modes appear are listed in Table 2 where they are compared with the 1-D model and experimental results. Fig.6(a) and 6(b) are both "to carrier" quarter wave modes, and show strong variation across the width of the device. 6(c) shows a "to reflector" quarter-wave, and predicts that the forces will be stronger nearer the centre of the chamber. This is observed in practice, although the pattern of force variation is more complex than the model predicts. This is probably due to poorly matched boundary conditions – both of the energy dissipation of the gasket, and the complex nature of the clamping that is not reflected in the model. The main uses of the model are to provide indications of the type of variation to be expected, and give insights into the causes of these variations. In particular we note that surface and plate-wave type mode shapes have a strong influence on lateral behaviour. In the future we will use the finite element models to develop designs that are less sensitive to geometric variations and material parameters to produce manipulation devices that produce more uniform action over a chamber area.

3 Enhancement of Microbead Assay

This section describes how the multimodal operation can be used to assist microbead based assays. In this example, a mixture of 6µm diameter streptavidin functionalised polystyrene beads (Bangs labs, CP01N) and non-functionalised fluorescent control beads (Invitrogen, P24671, 6µm diameter,Cy5.5 labelled) are driven against a glass reflector which has been functionalised with a PEG-biotin coating. The "to carrier" quarter-wave is then applied to

remove the unbound control beads. In a more realistic application, the beads could be replaced by bacteria, and an antibody functionalised surface used. The finite element modelling predicts weakening axial forces at the chamber edges and the existence of complex lateral variations, particularly for the "to-carrier" mode. These variations may also be aggravated by inlet channel geometry which results in asymmetric boundary conditions. However an area of approximately $1mm^2$ was found near the centre of the chamber where both the required acoustic modes were reasonably uniform. White light was coupled into the glass reflector through its end face such that an evanescent field was established close to the surface. This evanescent field illuminates any beads in direct contact with the reflector. An epifluorescent microscope was used to distinguish between the streptavidin beads and the fluorescent control beads.

The biotin surface functionalisation was performed as follows: Initially the glass slide surface was cleaned by sequentially immersing it with ultrasonic agitation in ethanol, isopropanol, then de-ionized water, 10 minutes at each step, with further rinsing in de-ionized water. The surface was activated by immersing the slide in a piranha etch for 15 minutes. Silanization was performed by immersing the slide for 3h in a 0.1% solution of 3-aminopropyl-trimethoxysilane at room temperature. Finally, the slide was soaked for three hours in a 0.2% solution of biotin-PEG-NHS, Mr 3400 (Creative PEGWorks, USA).

Drive voltages were set to 19Vpp. The strength of the radiation forces were measured using the force balance method described by Martin et al. [13] whereby drive voltage is reduced until the radiation force is just balanced by the sedimentation force. At 19Vpp, this predicts forces of approximately 4.1 and 10.1pN for the to-reflector and to-carrier modes respectively. These values have an estimated error of 8%, associated with the difficulty in distinguishing between a particle sedimenting very slowly and one still being held

After applying the "to reflector" quarter-wave, all beads were seen to reach the surface within 1s of activation (Fig.7.(a)). After a 90s delay to ensure bead capture, excitation was switched to the "to carrier" mode (Fig.7.(b)). Based on the images collected over a series of 5 repeated experiments, it was found that this removed 80% (±9%) of the control beads, while 90% (±6%) of the streptavidin beads remained attached to the surface. A short 0.5s burst of $2mms^{-1}$ flow through the chamber was sufficient to dislodge further Cy5.5 labelled control beads, such that 92% of them in total were removed. This compares to the case when no ultrasound was used, where even after 270s only a small proportion of the beads were seen to be in contact with the waveguide surface, the remainder possibly repelled by electrostatic forces. These results show that this technique could provide a new and useful type of rapid assay. It should be noted that no efforts were made to optimise the surfaces and experimental conditions to reduce non-specific binding to a level that would be necessary for practical assays – rather these experiments seek to show proof of concept.

4 Conclusion

In the device presented, both quarter-wavelength modes have been demonstrated and at frequencies which tally closely with modelled results. These modes have been shown to significantly enhance the immobilisation of functionalised beads, with all beads brought to the surface within 1s.

A 3-D finite element model incorporating both the piezoelectric and acoustic interactions has been verified against a layered device. Applying this to an axisymmetric model of the manipulator device we obtain useful insights into the action of the device. It predicts the type of lateral force variations that are observed experimentally, but further work to improve the way boundary conditions and damping are modelled is required before we can be confident in the modelled results. The model is sufficiently accurate to be useful in the future for developing designs that are less sensitive to geometric variations and material parameters, and to produce manipulation devices that produce more uniform action over a chamber area.

5 Acknowledgements

This work was supported by the EPSRC (grant EP/D03454X/1), DSTL, Point Source, and Genetix Ltd..

6 References

[1] N. Jaffrezic-Renault, C. Martelet, Y. Chevolot, and J.P. Cloarec, “Biosensors and bio-bar code assays based on biofunctionalized magnetic microbeads”, Sensors, vol. 7, pp. 589-614, 2007.

[2] M. Hill, Y. Shen and J. J. Hawkes, “Modelling of layered resonators for ultrasonic separation”, Ultrasonics, vol. 40, pp. 385-392, 2002.

[3] R. Krimholt, D. A. Leedom and G. L. Matthaei, “New Equivalent Circuits for Elementary Piezoelectric Transducers”, Electron. Lett,, vol. 6, pp. 398, 1970.

[4] A. Neild, S. Oberti, A. Haake, and J. Dual, "Finite element modeling of a microparticle manipulator", Ultrasonics, vol. 44, pp. e455-e460, 2006.

[5] O. Manneberg, B. Vanherberghen, J. Svennebring, H.M. Hertz, B. Onfelt, and M. Wiklund, “A three-dimensional ultrasonic cage for characterization of individual cells”, Applied Physics Letters, vol. 93, id. 063901, 2008.

[6] T. Lilliehorn, U. Simu, M. Nilsson, M. Almqvist, T. Stepinski, T. Laurell, J. Nilsson, and S. Johansson, “Trapping of microparticles in the near field of an ultrasonic transducer”, Ultrasonics, vol. 43, pp. 293-303, 2005.

[7] S. M. Hagsater, C. H. Westergaard, H. Bruus, and J. P. Kutter, "A compact viewing configuration for stereoscopic micro-PIV utilizing mm-sized mirrors," Experiments in Fluids, vol. 45, pp. 1015-1021, 2008.

[8] R. J. Townsend, M. Hill, N. R. Harris, and N. M. White, "Investigation of two-dimensional acoustic resonant modes in a particle separator", Ultrasonics, vol. 44, pp. e467-e471, 2006.

[9] ANSYS Inc., "ANSYS^{TM} Theory Reference Manual", Release 9.0, PA, USA, November 2004.

[10] L. E. Kinsler, A. E. Frey, A. B. Coppens, and J. V. Saunders, Fundamentals of acoustics, 3rd ed. New York: Wiley, 1982.

[11] L. P. Gor'kov, "On the forces acting on a small particle in an acoustical field in an ideal fluid", Sov. Phys. Dokl., vol. 6, pp. 773-5, 1962.

[12] M. Gröschl, "Ultrasonic separation of suspended particles - Part I: Fundamentals", Acustica, vol. 84, pp. 432-447, 1998.

[13] S. P. Martin, R. J. Townsend, L. A. Kuznetsova, K. A. J. Borthwick, M. Hill, M. B. McDonnell, and W. T. Coakley, "Spore and micro-particle capture on an immunosensor surface in an ultrasound standing wave system," Biosensors & Bioelectronics, vol. 21, pp. 758-767, 2005.

Fig.1. Multi-modal function of device showing force on beads, final location and pressure field for a) "to-reflector" mode; beads and immobilised bio-molecules move up to waveguide surface whereupon functionalised beads (○) will attach to the reflector surface, and b) "to-carrier" mode; unbound beads (●) are pulled away and towards the carrier layer surface.

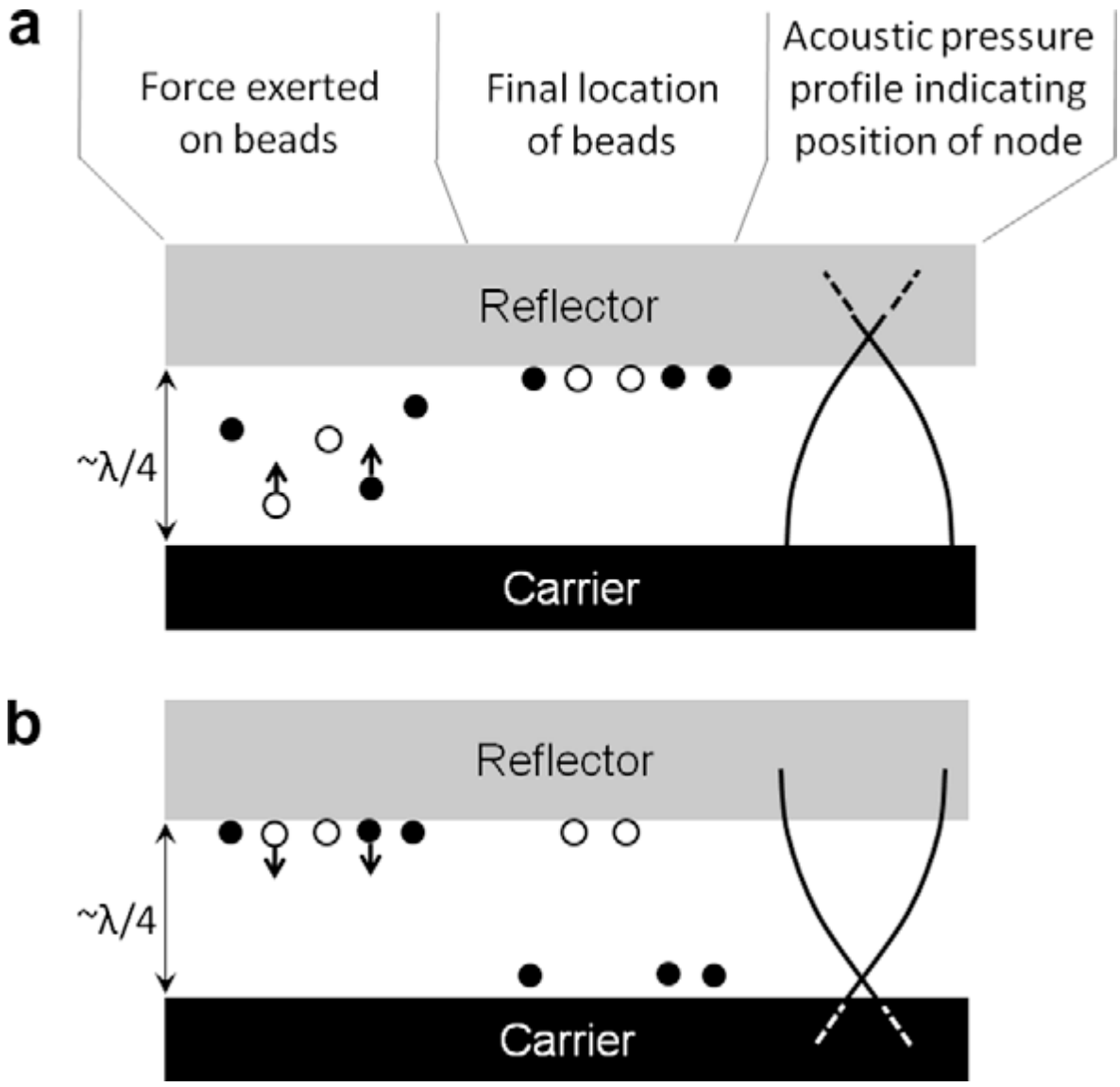

Fig.2. Photograph of particle manipulator device showing the main fluid chamber capped by a glass slide.

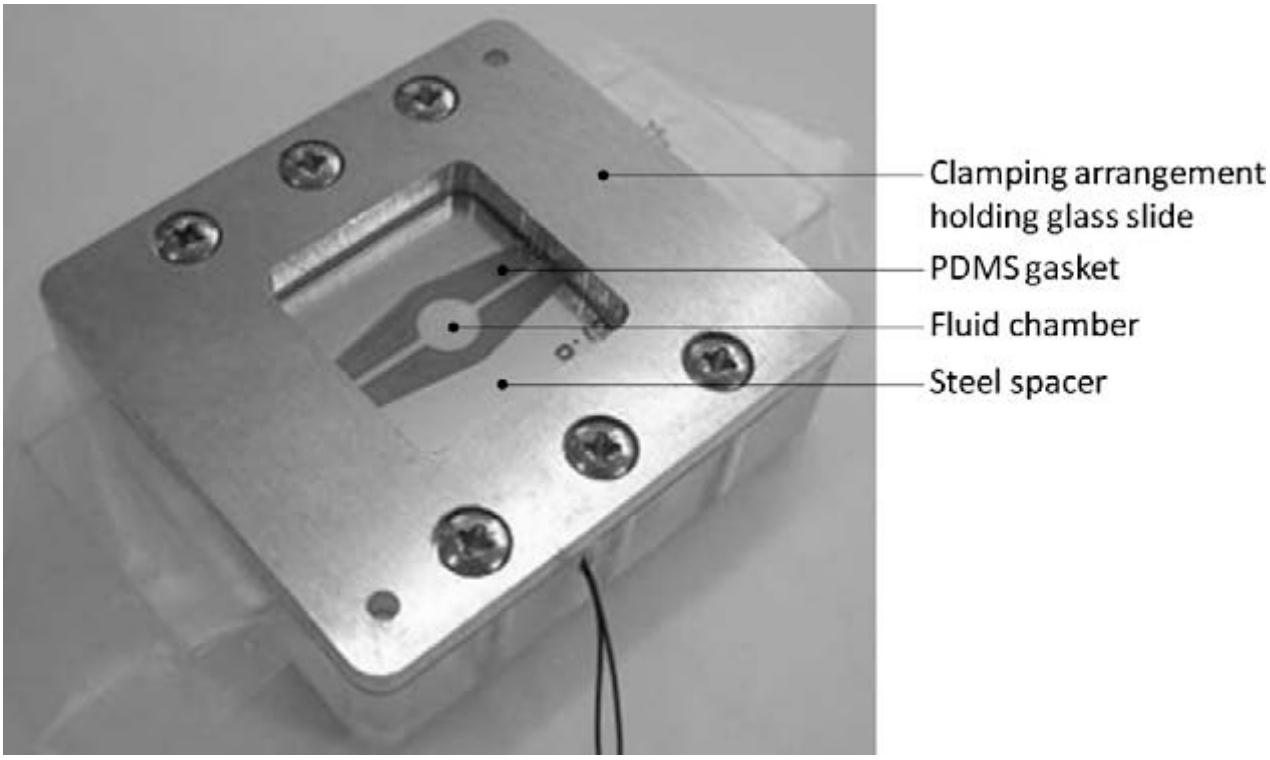

Fig.3. MATLAB 1-D model results for a) magnitude of electrical impedance and b) acoustic energy density within the fluid layer. Dashed lines correspond to predicted resonant modes at 1.572MHz and 1.700MHz.

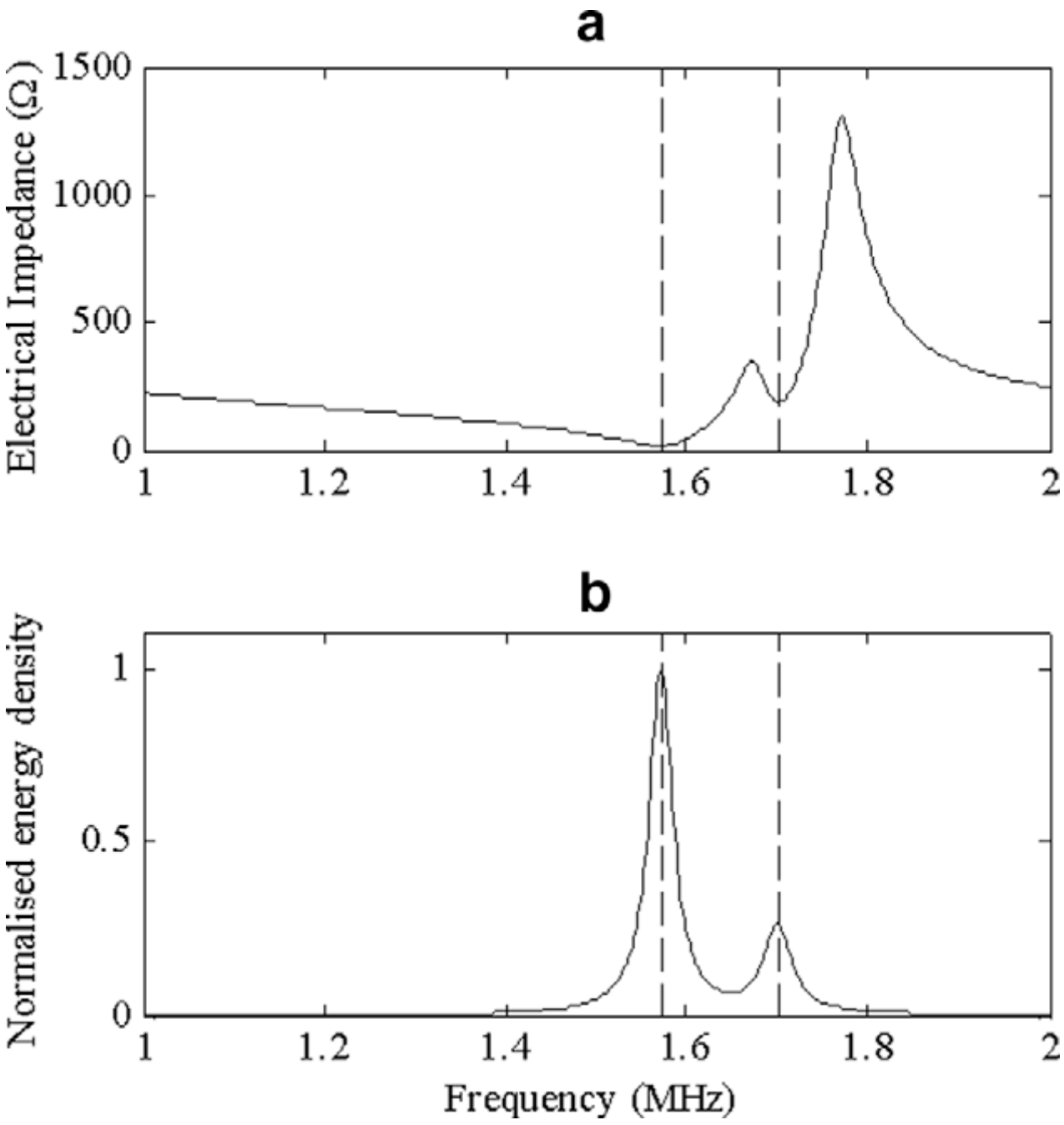

Fig.4. Predicted acoustic energy density for 1-d system and comparison between FE and transfer impedance models.

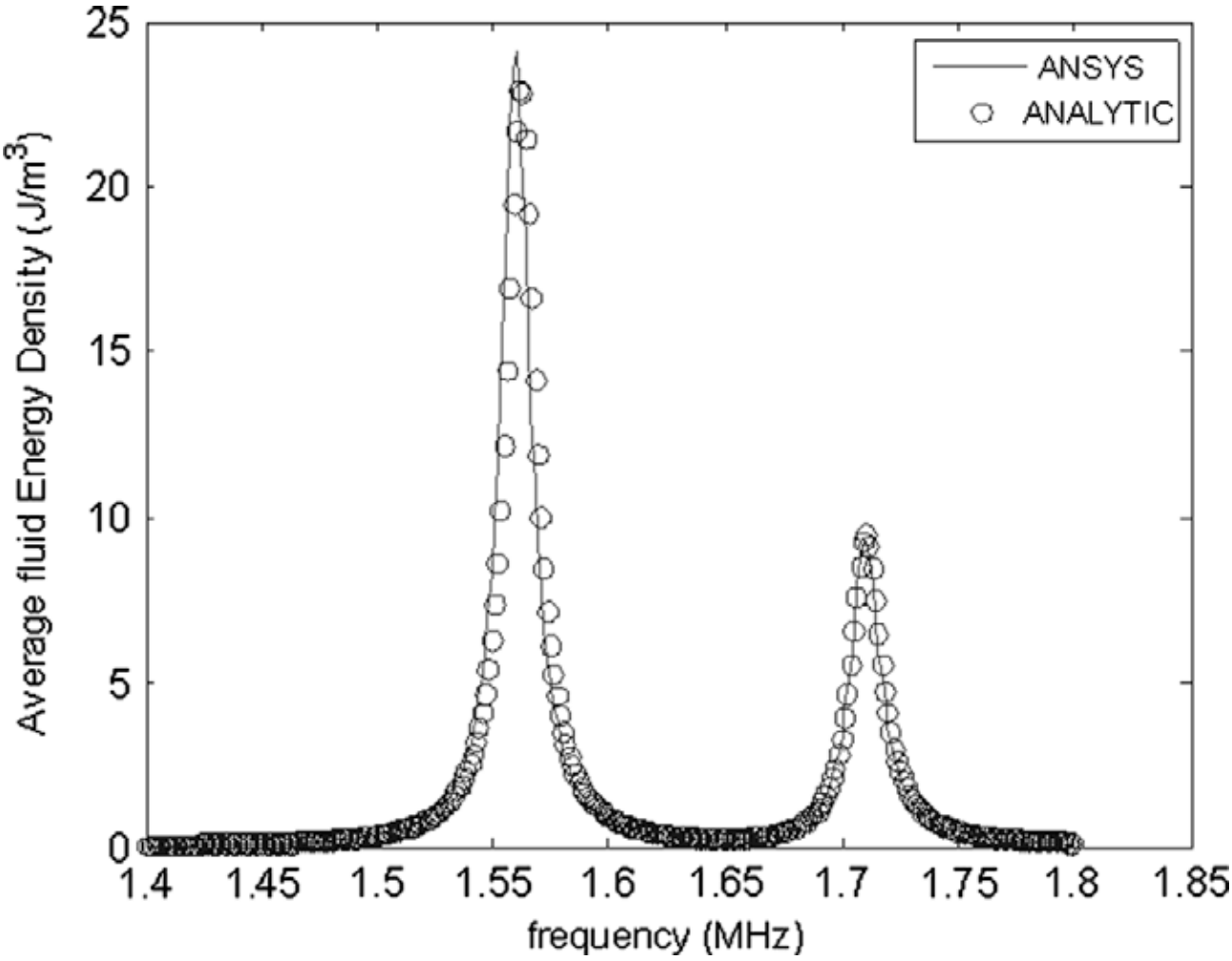

Fig.5. Construction of FE model (ANSYS).

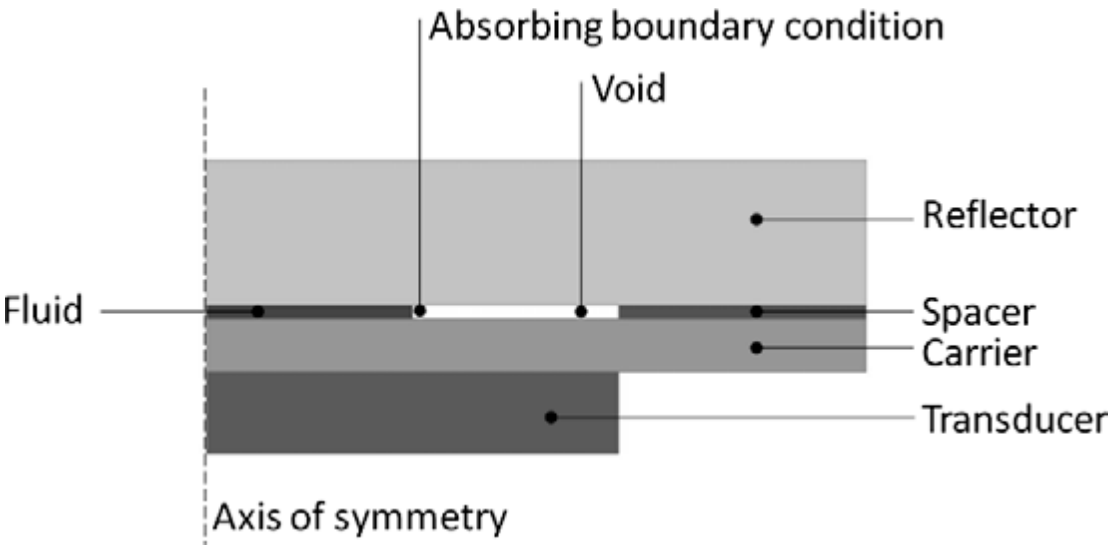

Fig.6. Plots of force potential in fluid layer elements (see Fig. 4) where black indicates agglomeration region for a) 1.55MHz “to carrier” quarter-wave, b) 1.61MHz “to carrier” quarter-wave and c) 1.72MHz “to reflector” quarter-wave.

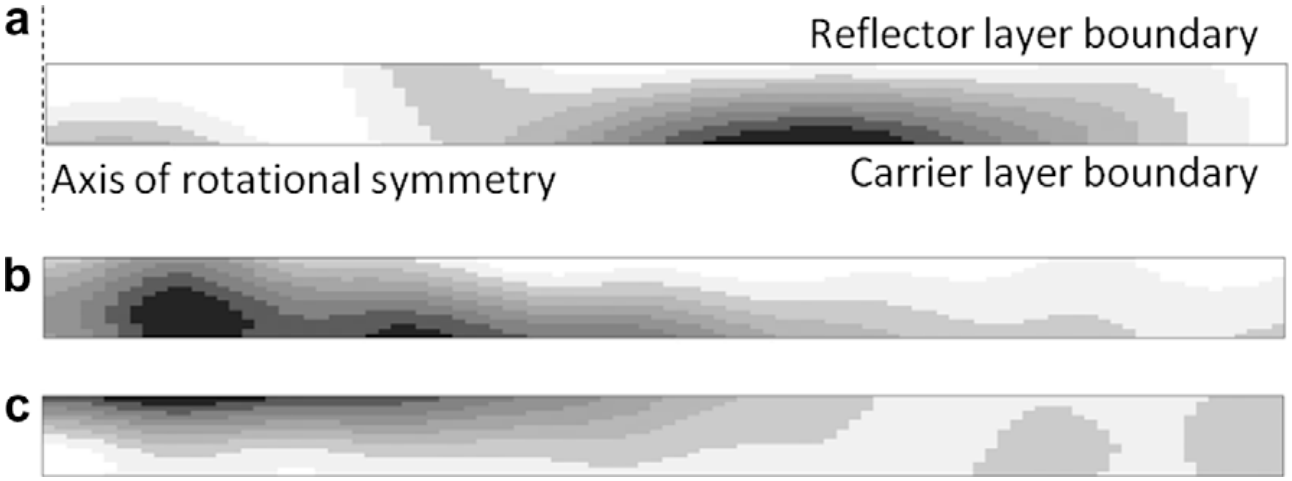

Fig.7. Microscope images of control and streptavidin coated beads located on reflector surface after a) initial application of “to reflector” quarter wave and b) subsequent application of “to carrier” quarter wave excitation.

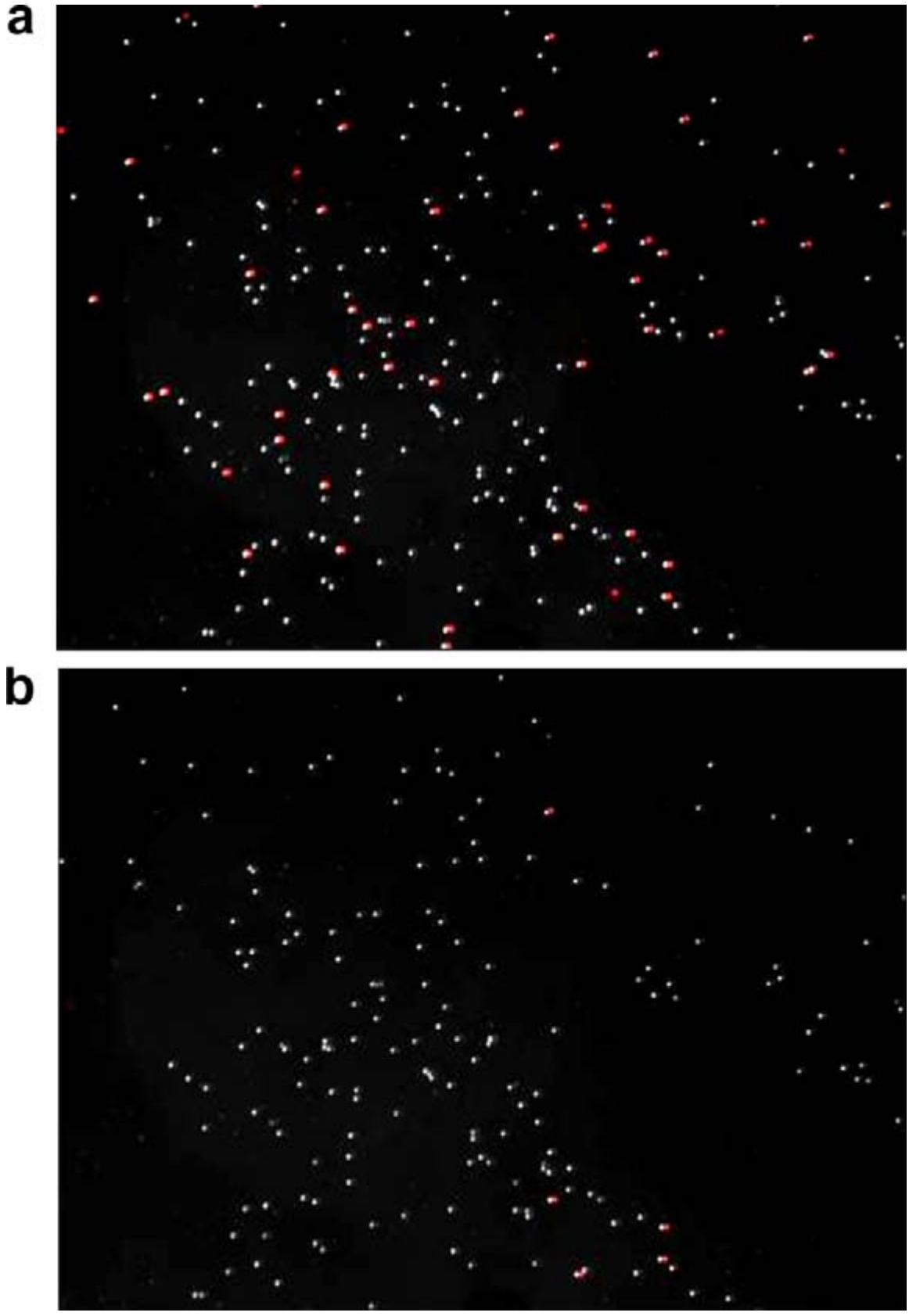

Table 1. Geometry of device

Layer	Material	Thickness (μm)	Density ($kg/m^{3)}$	Sonic velocity (m/s)
Transducer	PZ26	1000	7700	4529
Carrier	Alumina	650	3860	10520
Fluid	Water	162	1000	1480
Reflector	BK7 glass*	1762*	2500	5872

*Thickness and properties chosen for optical detection system.

Table 2. Frequencies of operation (MHz)

Mode	1-D Model (MATLAB)	FE Model (ANSYS)	Measured
“to-carrier”	1.572	1.55 & 1.61	1.508
“to-reflector”	1.700	1.72	1.712